

# Phonon scattering processes in molybdenum disulfide

HPSTAR  
712-2019

Cite as: Appl. Phys. Lett. **114**, 052102 (2019); doi: [10.1063/1.5082932](https://doi.org/10.1063/1.5082932)

Submitted: 26 November 2018 · Accepted: 11 January 2019 ·

Published Online: 5 February 2019



View Online



Export Citation



CrossMark

Zi-Yu Cao<sup>1,2,3</sup> and Xiao-Jia Chen<sup>3,a)</sup>

## AFFILIATIONS

<sup>1</sup>Key Laboratory of Materials Physics, Institute of Solid State Physics, Chinese Academy of Sciences, Hefei 230031, China

<sup>2</sup>University of Science and Technology of China, Hefei 230026, China

<sup>3</sup>Center for High Pressure Science and Technology Advanced Research, Shanghai 201203, China

<sup>a)</sup>Electronic mail: [xjchen@hpstar.ac.cn](mailto:xjchen@hpstar.ac.cn)

## ABSTRACT

Compared with graphene, 2H-MoS<sub>2</sub> possesses a non-zero bandgap and thus has an unlimited potential for electronic, spintronic, and optoelectronic applications. Understanding of the phonon scattering mechanisms is crucial to its device applications because the heat flow and transport are the basic processes functioning at various temperatures. So far, the knowledge of the phonon anharmonicity of 2H-MoS<sub>2</sub> is limited due to the availability from a narrow temperature range and the absence of the low frequency phonon information. Here, we report an experimental study on the temperature dependence of the frequency and line-width of 2H-MoS<sub>2</sub> by Raman scattering over a wide temperature range from 2.2 to 1000 K and down to the wavenumber of 10 cm<sup>-1</sup>. The cubic anharmonicity is found to be dominant at low temperatures, and quartic anharmonicity predominates at high temperatures. The obtained shear mode seems insensitive to the anharmonic effects. The damping effects are discussed based on the available experimental data. These phonon scattering behaviors of 2H-MoS<sub>2</sub> are of great help to the future nanodevice developments and applications.

Published under license by AIP Publishing. <https://doi.org/10.1063/1.5082932>

Two-dimensional materials possess characters such as strong intra-layer bonding with weak inter-layer attraction. These natures bring remarkable properties which could put two-dimensional materials into practice. One of the most exposed materials of such a kind is graphene,<sup>1</sup> which updates the interest in inorganic materials with its unique electronic<sup>2</sup> and optical<sup>3-5</sup> applications and high mobility.<sup>6</sup> However, the absence of the bandgap is a limitation for its electronic applications, especially as transistors. In contrast, the transition-metal dichalcogenides (TMDs), quasi-2D materials with distinct structures and unique physical properties, possess non-zero bandgaps that could also be tuned.<sup>7-9</sup> An extensively investigated member of TMDs is 2H-MoS<sub>2</sub>. Recent experiments have reported that the mobility of monolayer 2H-MoS<sub>2</sub> shows several times larger than traditional thin silicon films and graphene nanoribbons.<sup>2,10</sup> Because of the missing of the inversion symmetry,<sup>11</sup> 2H-MoS<sub>2</sub> has an effect associated with the strong coupling of spin and valley degrees of freedom. This makes 2H-MoS<sub>2</sub> as a good candidate for various valley electronic and optoelectronic applications.<sup>12</sup> Furthermore, the essentially strong spin-orbit

coupling in 2H-MoS<sub>2</sub> opens opportunities for building blocks in spintronic applications.<sup>13</sup> However, the devices with an extremely high degree of integration are impressionable to the heat transfer and phonon behaviors. It is important to fundamentally comprehend the heat dissipation. The lattice anharmonicity reflects the intrinsic phonon scattering which is related to the thermal conductivity characteristic. The study on the anharmonic phonon in 2H-MoS<sub>2</sub> is extremely important before putting 2H-MoS<sub>2</sub> into practice.

Raman spectroscopy is a powerful tool which can directly provide a great deal of information about the optical phonon near the center of the Brillouin zone. Both the frequency and the full width at half maximum (FWHM) of a vibrational mode carry the information concerning the lattice anharmonicity. The anharmonic effects have been widely investigated by the temperature dependence of the Raman spectra on silicon, black phosphorus, graphene, and various 2D-materials.<sup>14-22</sup> In contrast, this kind of investigation on 2H-MoS<sub>2</sub> was reported sparsely.<sup>23-26</sup> Previous investigations on the temperature dependence of the frequency of 2H-MoS<sub>2</sub> were carried on over

a temperature range between 83 K and 550 K.<sup>23–25</sup> A linear temperature dependence of the frequency of the Raman modes was observed. However, the FWHM variation with temperature was ignored. Taube *et al.*<sup>26</sup> indeed observed a temperature dependence of the nonlinear frequency of 2H-MoS<sub>2</sub> over a temperature range from 70 to 350 K. The narrow temperature range limited the identification of the phonon scattering mechanisms. The extreme temperature conduction is indispensable for the investigation of the lattice anharmonicity. Both the frequency and FWHM should saturate at low temperatures. The higher order anharmonicity may dominate at high temperature. Meanwhile, the temperature dependence of the frequency and FWHM of the low frequency mode has never been reported because of the overreaction of the Rayleigh scattering. Complete Raman spectra with a wide temperature range for 2H-MoS<sub>2</sub> are thus highly desired.

In this work, the temperature dependence of the Raman spectra of 2H-MoS<sub>2</sub> is investigated over a temperature range from 2.2 to 1000 K. The changes in the frequency and FWHM with the temperature of the Raman modes are clearly observed. Intrinsic phonon scattering mechanisms are discussed based on the obtained experimental data. Our results provide direct experimental evidence for the anharmonic effects in 2H-MoS<sub>2</sub>. This work offers a complete understanding of the heat dissipation in this TMD which is crucial to nanoscale devices.

High-quality single crystal 2H-MoS<sub>2</sub> was purchased from HQGraphene. A dimension of 50  $\mu\text{m}$   $\times$  50  $\mu\text{m}$   $\times$  4  $\mu\text{m}$  was used for the Raman scattering experiment. A He continuous flowing cryostat was used for the low-temperature (2.2–300 K) part. The temperature was measured using Pt resistance sensors close to the sample with a typical precision of  $\pm 0.5$  K. For the high-temperature (300–1000 K) Raman scattering experiment, 2H-MoS<sub>2</sub> was placed into a diamond shelf. The resistance heater was twined around the diamond shelf and powered by a current source. A K-type thermocouple was used to determine the temperature with a typical precision of  $\pm 1$  K. The entire device was immersed into a shielding gas (97 vol. % argon + 3 vol. % hydrogen) continuous flowing device to avoid being oxidized. The Raman spectra were measured using a single stage spectrograph equipped with an array thermoelectrically cooled charge coupled device detector. The 488 excitation was used to illuminate a circle with a diameter of 2  $\mu\text{m}$  on the new stripping shining surface of 2H-MoS<sub>2</sub>. The Raman spectra were collected with a laser power down to 1.0 mw to avoid laser the heating effect. The heating effects are quantified by the ratio of the anti-Stokes to Stoke Raman intensity at room temperature and found to be 3–12 K.

Raman spectroscopy is an effective method to detect the phonon vibrations and the anharmonic effects. The irreducible representations of the phonon modes in 2H-MoS<sub>2</sub> are  $A_{1g} + 2B_{2g} + E_{1g} + 2E_{2g} + 2A_{2u} + B_{1u} + 2E_{1u} + E_{2u}$ . Among them  $A_{1g}$ ,  $E_{1g}$ ,  $E_{2g}^1$ , and  $E_{2g}^2$  modes are Raman active modes. The insets of Fig. 1 are the sketches of the active vibrational modes of 2H-MoS<sub>2</sub>. In TMDs, the  $E_{1g}$  mode is always weak due to its small Raman scattering cross section.<sup>3</sup> At room temperature, the Raman active modes are observed at 34.7 ( $E_{2g}^2$ ), 385.6 ( $E_{2g}^1$ ), and 410.9 ( $A_{1g}$ )  $\text{cm}^{-1}$  with FWHMs of 2.3 ( $E_{2g}^2$ ), 2.8 ( $E_{2g}^1$ ), and 3.1 ( $A_{1g}$ )

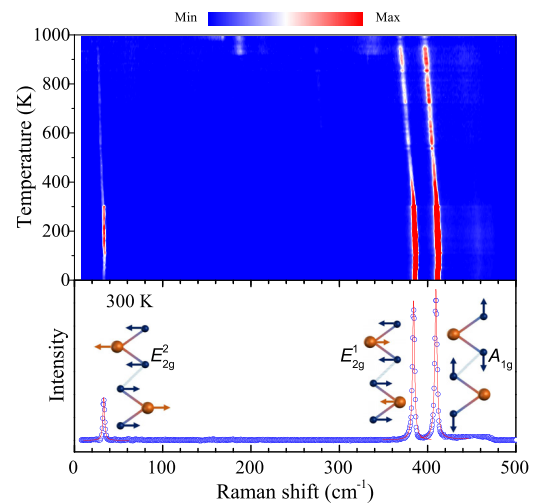


**FIG. 1.** The upper panel is the 2D presentation in the Raman frequency–temperature coordinates, and the bottom panel is a typical Raman spectrum at room temperature. Each vibrational mode was fitted with the Lorentz formula (red line) to the data points in open circles.

$\text{cm}^{-1}$ , respectively. Our observation of the Raman spectra of 2H-MoS<sub>2</sub> at room temperature agrees very well with previous publications.<sup>9,27,28</sup> This also indicates the high quality of the single crystal.

A strong temperature-dependent Raman scattering character has been found for 2H-MoS<sub>2</sub>. The upper panel of Fig. 1 shows the evolution of the Raman spectra over a wide temperature range from 2.2 to 1000 K. At the temperature above 940 K, some unknown peaks appear in Raman spectra (upper panel of Fig. 1). This indicates that 2H-MoS<sub>2</sub> is oxidized. Below 1000 K, the Raman vibrational mode in 2H-MoS<sub>2</sub> are still clear. We thus analyze the Raman spectrum at the temperature below 1000 K to define the phonon scattering processes. The  $E_{2g}^1$  and  $A_{1g}$  modes in 2H-MoS<sub>2</sub> observably soften and slightly broaden with increasing temperature, especially above 400 K. From 2.2 to 1000 K, the frequency of the  $E_{2g}^1$  mode decreases from 387.4 to 369.7  $\text{cm}^{-1}$  and the  $A_{1g}$  mode changes from 412.5 to 396.4  $\text{cm}^{-1}$ . Meanwhile, the FWHM of the  $E_{2g}^1$  mode broadens from 2.0 to 5.7  $\text{cm}^{-1}$  and the  $A_{1g}$  mode broadens from 2.3 to 5.9  $\text{cm}^{-1}$ . In contrast, the behavior of the shear mode is insensitive to temperature. The frequency of the  $E_{2g}^2$  mode shows a slight redshift, and the change in the FWHM is indistinguishable. Moreover, the temperature dependence of the nonlinear frequency shifts can be detected at low temperature. At the temperature above 150 K, the frequency of the vibration modes varies linearly with temperature. The first-order temperature coefficient at the temperature above 150 K of the  $E_{2g}^2$ ,  $E_{2g}^1$ , and  $A_{1g}$  modes is  $-0.0075$ ,  $-0.191$ , and  $-0.0175$   $\text{cm}^{-1}/\text{K}$ , respectively. The temperature coefficient is slightly higher than that in the previous report.<sup>27,28</sup> It may be because of the difference of the thickness of the sample. The anharmonic interactions and the thermal expansion often play important roles in the change of the frequency and FWHM in the Raman spectra.<sup>14,29,30</sup> However, in 2H-

MoS<sub>2</sub>, the thermal expansion coefficient was reported to be 10<sup>-5</sup> to 10<sup>-6</sup> in magnitudes.<sup>31</sup> The small thermal expansion coefficient brings about little contribution to the change in the frequency and thus can be neglected. The observed change in Raman spectra with temperature is mainly governed by the anharmonic potential. Based on the Klemens-Hart-Aggarwal-Lax model,<sup>32,33</sup> Balkanski *et al.*<sup>14</sup> developed a semi-quantitative formula to comprehend the phonon behavior with the cubic and/or quartic anharmonicity of the lattice potential. The anharmonicity could be concluded through this model by the temperature dependence of the Raman frequency and FWHM over a wide temperature range. The cubic anharmonicity is characterized as

$$\omega(T) = \omega_0 + A \left[ 1 + \frac{2}{e^x - 1} \right]. \quad (1)$$

Moreover, if the quartic anharmonicity is concerned, the functional form is upgraded to

$$\omega(T) = \omega_0 + A \left[ 1 + \frac{2}{e^x - 1} \right] + B \left[ 1 + \frac{3}{e^y - 1} + \frac{3}{(e^y - 1)^2} \right], \quad (2)$$

where  $x = \hbar\omega_0/2k_B T$ ,  $y = \hbar\omega_0/3k_B T$ ,  $\omega_0$  is the phonon energy at  $T = 0$  K,  $\hbar$  is the reduced Planck constant, and  $k_B$  is the Boltzmann constant. Coefficients A and B are constants representing the contributions of the cubic and quartic anharmonicity of the lattice potential. The upper panels of Fig. 2 exhibit the detailed calculation of the frequencies of all the observed modes. The nonlinear frequency shifts are clearly observed. The red dashed lines represent the frequencies of the Raman modes calculated with the cubic anharmonicity. The fitting curves with the cubic anharmonicity match well with the data points at low temperatures. However, they seriously diverge the experimental data points at high temperatures. This deviation at high temperatures is due to the primary contribution of the four-phonon process. Equation (2) is used to fit the temperature dependence of the frequency presented in the upper panels of Fig. 2. The constants A and B (the values of A and B are listed in Table I) are chosen

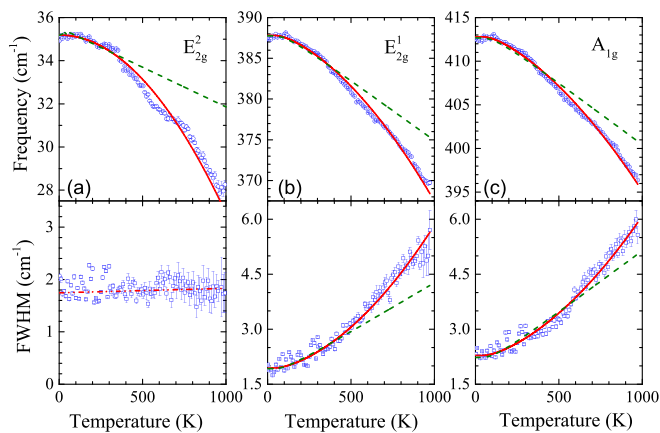


**FIG. 2.** The frequency and FWHM of the  $E_{2g}^2$  (a),  $E_{2g}^1$  (b), and  $A_{1g}$  (c) modes versus temperature. The dashed line gives the theoretical fitting using the three phonon process, and the solid red line represents the cubic and quartic anharmonicity. The red dot-dashed line is the linear fit to the FWHM of the  $E_{2g}^2$  mode.

appropriately so that the calculated curves (solid red line) agree well with the experimental data. The cubic anharmonicity coefficient of the  $A_{1g}$  mode ( $-1.26 \text{ cm}^{-1}$ ) is stronger than the coefficient in the  $E_{2g}^1$  mode ( $-1.05 \text{ cm}^{-1}$ ). In contrary, the quartic anharmonicity coefficient of the  $A_{1g}$  mode ( $-0.14 \text{ cm}^{-1}$ ) is weaker than the coefficient in the  $E_{2g}^1$  mode ( $-0.16 \text{ cm}^{-1}$ ). The shear mode shows a minimum correlation with the anharmonic effects with  $A = -0.03 \text{ cm}^{-1}$  and  $B = -0.001 \text{ cm}^{-1}$ .

The lower panels of Fig. 2 illuminate the FWHM behavior as a function of temperature. The temperature dependence of the intrinsic phonon scattering is performed by using the following functional form:<sup>14</sup>

$$\Gamma(T) = \Gamma_0 + C \left[ 1 + \frac{2}{e^x - 1} \right] + D \left[ 1 + \frac{3}{e^y - 1} + \frac{3}{(e^y - 1)^2} \right], \quad (3)$$

where  $\Gamma_0$  is the inherent FWHM of the sample. The three-phonon processes (red dashed lines) are fitted by omitting the parameter D. The temperature dependence of the FWHM of the  $E_{2g}^1$  mode is in accordance with the three-phonon process at the temperatures up to 400 K and the  $A_{1g}$  mode up to 600 K but deviates at higher temperatures. Four-phonon processes are predominant at higher temperatures. Equation (3) shows that the cubic and quartic anharmonicity matches well with the experimental data. The behaviors of the anharmonic effects from the temperature dependence of the FWHM are similar to those drawn from the temperature of the frequency, especially for the  $E_{2g}^1$  and  $A_{1g}$  modes. The best fitting coefficients are found to be  $C = 0.13 \text{ cm}^{-1}$  and  $D = 0.04 \text{ cm}^{-1}$  for the  $E_{2g}^1$  mode and  $C = 0.20 \text{ cm}^{-1}$  and  $D = 0.03 \text{ cm}^{-1}$  for the  $A_{1g}$  mode. However, the FWHM of the shear mode is almost independent with the temperature.

Figure 3 shows an abridged general view of the phonon scattering processes in the phonon dispersion curve.<sup>34,35</sup> Generally speaking, the four-phonon process has a much lower scattering probability than the three-phonon process since the former is in higher order. However, at high temperatures, a much great number of four-phonon processes take part in the phonon scattering processes because of the allowance of the momentum and energy selection rules.<sup>16</sup> Therefore, the four-phonon process is comparable with the three-phonon process and even becomes predominant one at high temperatures. Different phonon branches are coupled by the anharmonic effect with the law of the conservation of energy and momentum. The optical phonon shows high energy around the  $\Gamma$  point ( $280\text{--}470 \text{ cm}^{-1}$ ). Three and most of the four phonon processes (except redistribution processes) containing only optical phonons are forbidden because of they do not match with the energy coordinate. The anharmonic effect largely reflects the

**TABLE I.** Phonon damping constants of the Raman modes in 2H-MoS<sub>2</sub>.

Mode	A (cm <sup>-1</sup> )	B (cm <sup>-1</sup> )	C (cm <sup>-1</sup> )	D (cm <sup>-1</sup> )
$E_{2g}^2$	-0.03	-0.001	...	...
$E_{2g}^1$	-1.05	-0.16	0.13	0.04
$A_{1g}$	-1.26	-0.14	0.20	0.03

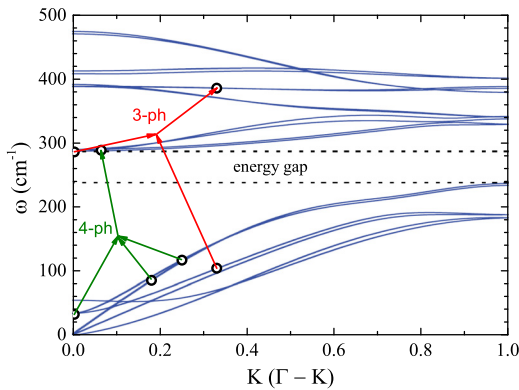


**FIG. 3.** Schematic diagram of the phonon scattering processes in  $2H\text{-MoS}_2$ . The red arrows indicate a three-phonon process, and the green arrows show a four-phonon process.

coupling between the optical phonons and acoustic phonons. The acoustic phonons which have nonzero group velocity contribute to the thermal conductivity. The enhancement of the anharmonic effect increases the odds of the collision between phonons and leads to the reduction of the phonon lifetime accordingly. Therefore, the anharmonic effect extracted from Raman spectra is closely bound up with the thermal conductivity.

The total thermal conductivity is divided into electronic parts and lattice components. The carrier concentration of  $2H\text{-MoS}_2$  at room temperature is  $10^{17}\text{cm}^{-3}$  in magnitude.<sup>36</sup> The excessive small carrier concentration in  $2H\text{-MoS}_2$  is attributed to low electronic thermal conductivity. The lattice thermal conductivity thus governs the heat transport. The thermal conductivity [see Fig. 4(d)] of  $2H\text{-MoS}_2$  has already been reported.<sup>24,37–43</sup> The thermal conductivity enhances as the temperature is increased up to 100 K. However, a hump is observed reversing the slope in the temperature interval below the maximum. Above 100 K, the thermal conductivity keeps reducing with increasing temperature. The anharmonic effect will reduce the mean free path and thus also account for the hump shown in thermal conductivity. At low temperatures, the weak anharmonic effect results in a long phonon mean free path. However, the long phonon mean free path is sensitive to the defects. In this regime, only few phonons participate in the heat transport. For the temperatures below 100 K, the reduction of the thermal conductivity with decreasing temperature originates from the specific heat. As the temperature is increased, the anharmonic effect is gradually enhanced. The shorter phonon mean free path is not susceptible to the defects. On the other hand, the number of phonons is increased. Phonon-phonon scattering is primary at temperatures above 100 K. Caused by the anharmonic effects, the change in the frequency and the FWHM in Raman spectra directly reflects the damping effect.<sup>14</sup> In general, the damping constant is reciprocal of the phonon lifetime,<sup>44</sup> and the phonon lifetime is proportional to the thermal conductivity. Consequently, the temperature dependences of the frequency and FWHM (especially the FWHM) are inversely proportional to the lattice thermal conductivity.<sup>44</sup> The devices with an

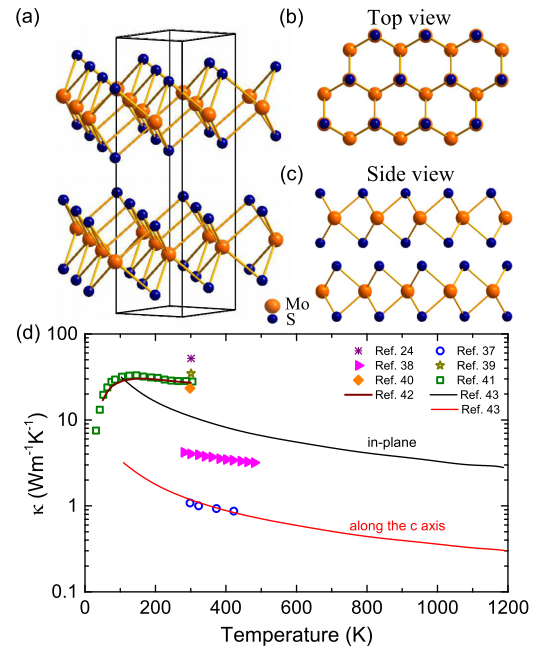


**FIG. 4.** (a)–(c) Three-dimensional schematic representation of a typical  $2H\text{-MoS}_2$  structure with the S atoms in dark blue and the Mo atoms in orange. (d) Temperature dependence of the thermal conductivity of  $2H\text{-MoS}_2$ . The open dots are experimental works. The solid lines and solid dots are theoretical works.

extremely high degree of integration are impressionable to the heat transfer. A proper regulation of the heat transfer improves the stability of the nanointegrated devices. The heat management relies on the phonon scattering behavior. The lattice anharmonicity reflects the intrinsic phonon scattering which is related to the thermal conductivity characteristic. The study on the anharmonic phonon in  $2H\text{-MoS}_2$  is extremely important for designing various nanoelectronic devices.

In summary, the anharmonic effects including three phonon and four phonon processes have been examined in  $2H\text{-MoS}_2$ . For the  $E_{2g}^1$  and  $A_{1g}$  modes, three phonon processes are the dominant processes at low temperatures. However, at high temperatures, the four-phonon processes are comparable to the three-phonon processes or even become predominant ones. On the other hand, the  $E_{2g}^2$  mode shows a little correlation with the anharmonic effects. In Raman spectra, the behaviors of the  $E_{2g}^1$  and  $A_{1g}$  modes are attributed to the lattice thermal conductivity most. Our results support the existence of the anharmonic effects in  $2H\text{-MoS}_2$ . This work fundamentally comprehends the heat dissipation which is crucial to nanointegrated devices.

## REFERENCES

- <sup>1</sup>K. S. Novoselov, A. K. Geim, S. V. Morozov, D. Jiang, M. I. Katsnelson, I. V. Grigorieva, S. V. Dubonos, and A. A. Firsov, "Two-dimensional gas of massless Dirac fermions in graphene," *Nature (London)* **438**, 197 (2005).
- <sup>2</sup>B. Radisavljevic, A. Radenovic, J. Brivio, V. Giacometti, and A. Kis, "Single-layer  $\text{MoS}_2$  transistors," *Nat. Nanotechnol.* **6**, 147 (2011).
- <sup>3</sup>Q. H. Wang, K. K. Zadeh, A. Kis, J. N. Coleman, and M. S. Strano, "Electronics and optoelectronics of two-dimensional transition metal dichalcogenides," *Nat. Nanotechnol.* **7**, 699 (2012).

- <sup>4</sup>D. J. Late, U. Maitra, L. S. Panchakarla, U. V. Waghmare, and C. N. R. Rao, "Temperature effects on the Raman spectra of graphenes: Dependence on the number of layers and doping," *J. Phys.: Condens. Matter* **23**, 055303 (2011).
- <sup>5</sup>A. S. Pawbake, K. K. Mishra, L. G. B. Machunoc, R. V. Gelamoc, T. R. Ravindranb, C. S. Rout, and D. J. Late, "Temperature and pressure dependent Raman spectroscopy of plasma treated multilayer graphene nanosheets," *Diamond Relat. Mater.* **84**, 146 (2018).
- <sup>6</sup>K. I. Bolotin, K. J. Sikes, Z. Jiang, M. Klima, G. Fudenberg, J. Hone, P. Kim, and H. L. Stormer, "Ultra-high electron mobility in suspended graphene," *Solid State Commun.* **146**, 351 (2008).
- <sup>7</sup>K. F. Mak, C. Lee, J. Hone, J. Shan, and T. F. Heinz, "Atomically thin MoS<sub>2</sub>: A new direct-gap semiconductor," *Phys. Rev. Lett.* **105**, 136805 (2010).
- <sup>8</sup>J. T. Ye, Y. J. Zhang, R. Akashi, M. S. Bahramy, R. Arita, and Y. Iwasa, "Superconducting dome in a gate-tuned band insulator," *Science* **338**, 1193 (2012).
- <sup>9</sup>Z. Y. Cao, J. W. Hu, A. F. Goncharov, and X. J. Chen, "Nontrivial metallic state of molybdenum disulfide," *Phys. Rev. B* **97**, 214519 (2018).
- <sup>10</sup>Y. Yoon, K. Ganapathi, and S. Salahuddin, "How good can monolayer MoS<sub>2</sub> transistors be?," *Nano Lett.* **11**, 3768 (2011).
- <sup>11</sup>H. Zeng, J. F. Dai, W. Yao, D. Xiao, and X. D. Cui, "Valley polarization in MoS<sub>2</sub> monolayers by optical pumping," *Nat. Nanotechnol.* **7**, 490 (2012).
- <sup>12</sup>D. Xiao, W. Yao, and Q. Niu, "Valley-contrasting physics in graphene: Magnetic moment and topological transport," *Phys. Rev. Lett.* **99**, 236809 (2007).
- <sup>13</sup>Z. Y. Zhu, Y. C. Cheng, and U. Schwingenschlögl, "Giant spin-orbit-induced spin splitting in two-dimensional transition-metal dichalcogenide semiconductors," *Phys. Rev. B* **84**, 153402 (2011).
- <sup>14</sup>M. Balkanski, R. F. Wallis, and E. Haro, "Anharmonic effects in light scattering due to optical phonons in silicon," *Phys. Rev. B* **28**, 1928 (1983).
- <sup>15</sup>B. C. Johnson, B. Haberl, J. E. Bradby, J. C. McCallum, and J. S. Williams, "Temperature dependence of Raman scattering from the high-pressure phases of Si induced by indentation," *Phys. Rev. B* **83**, 235205 (2011).
- <sup>16</sup>T. L. Feng and X. L. Ruan, "Quantum mechanical prediction of four-phonon scattering rates and reduced thermal conductivity of solids," *Phys. Rev. B* **93**, 045202 (2016).
- <sup>17</sup>J. J. Lin, L. W. Guo, Q. S. Huang, Y. P. Jia, K. Li, X. F. Lai, and X. L. Chen, "Anharmonic phonon effects in Raman spectra of unsupported vertical graphene sheets," *Phys. Rev. B* **83**, 125430 (2011).
- <sup>18</sup>D. J. Late, "Temperature dependent phonon shifts in few-layer black phosphorus," *ACS Appl. Mater. Interfaces* **7**, 5857 (2015).
- <sup>19</sup>M. Thripuranthaka and D. J. Late, "Temperature dependent phonon shifts in single-layer WS<sub>2</sub>," *ACS Appl. Mater. Interfaces* **6**, 1158 (2014).
- <sup>20</sup>A. S. Pawbake, A. Date, S. R. Jadhkar, and D. J. Late, *ChemistrySelect* **1**, 5380 (2016).
- <sup>21</sup>M. K. Jana, A. Singh, D. J. Late, C. R. Rajamathi, K. Biswas, C. Felser, U. V. Waghmare, and C. N. R. Rao, "A combined experimental and theoretical study of the structural, electronic and vibrational properties of bulk and few-layer Td-WTe<sub>2</sub>," *J. Phys.: Condens. Matter* **27**, 285401 (2015).
- <sup>22</sup>D. J. Late, "Temperature-dependent phonon shifts in atomically thin MoTe<sub>2</sub> nanosheets," *Appl. Mater. Today* **5**, 98 (2016).
- <sup>23</sup>S. Najmaei, P. M. Ajayan, and J. Lou, "Quantitative analysis of the temperature dependency in Raman active vibrational modes of molybdenum disulfide atomic layers," *Nanoscale* **5**, 9758 (2013).
- <sup>24</sup>S. Sahoo, A. P. S. Gaur, M. Ahmadi, M. J.-F. Guinel, and S. Katiyar, "Temperature-dependent Raman studies and thermal conductivity of few-layer MoS<sub>2</sub>," *J. Phys. Chem. C* **117**, 9042 (2013).
- <sup>25</sup>N. A. Lanzillo, A. G. Birdwell, M. Amani, F. J. Crowne, P. B. Shah, S. Najmaei, Z. Liu, P. M. Ajayan, J. Lou, M. Dubey, S. K. Nayak, and T. P. O'Regan, "Temperature-dependent phonon shifts in monolayer MoS<sub>2</sub>," *Appl. Phys. Lett.* **103**, 093102 (2013).
- <sup>26</sup>A. Taube, J. Judek, C. Jastrzebski, A. Duzynska, K. Świtekowski, and M. Zdrojek, "Temperature-dependent nonlinear phonon shifts in a supported MoS<sub>2</sub> monolayer," *ACS Appl. Mater. Interfaces* **6**, 8959 (2014).
- <sup>27</sup>M. Thripuranthaka, R. V. Kashid, C. S. Rout, and D. J. Late, "Temperature dependent Raman spectroscopy of chemically derived few layer MoS<sub>2</sub> and WS<sub>2</sub> nanosheets," *Appl. Phys. Lett.* **104**, 081911 (2014).
- <sup>28</sup>A. S. Pawbake, M. S. Pawar, S. R. Jadhkar, and D. J. Late, "Large area chemical vapor deposition of monolayer transition metal dichalcogenides and their temperature dependent Raman spectroscopy studies," *Nanoscale* **8**, 3008 (2016).
- <sup>29</sup>Z. Dohčević-Mitrović, Z. V. Popović, and M. Šćepanović, "Anharmonicity effects in nanocrystals studied by Raman scattering spectroscopy," *Acta Phys. Pol. A* **116**, 36 (2009).
- <sup>30</sup>L. C. Chen, Z. Y. Cao, H. Yu, B. B. Jiang, L. Su, L. D. Chen, and X. J. Chen, "Phonon anharmonicity in thermoelectric palladium sulfide by Raman spectroscopy," *Appl. Phys. Lett.* **113**, 022105 (2018).
- <sup>31</sup>C. K. Gan and Y. Y. F. Liu, "Direct calculation of the linear thermal expansion coefficients of MoS<sub>2</sub> via symmetry-preserving deformations," *Phys. Rev. B* **94**, 134303 (2016).
- <sup>32</sup>P. G. Klemens, "Anharmonic decay of optical phonons," *Phys. Rev.* **148**, 845 (1966).
- <sup>33</sup>T. R. Hart, "Temperature dependence of Raman scattering in silicon," *Phys. Rev. B* **1**, 638 (1970).
- <sup>34</sup>A. Molina-Sánchez and L. Wirtz, "Phonons in single-layer and few-layer MoS<sub>2</sub> and WS<sub>2</sub>," *Phys. Rev. B* **84**, 155413 (2011).
- <sup>35</sup>N. Wakabayashi, H. G. Smith, and R. M. Nicklow, "Lattice dynamics of hexagonal MoS<sub>2</sub> studied by neutron scattering," *Phys. Rev. B* **12**, 659 (1975).
- <sup>36</sup>S. H. Ei-Mahblawy and B. L. Evans, "Temperature dependence of the electrical conductivity and hall coefficient in 2H-MoS<sub>2</sub>, MoSe, WSe, and MoTe," *Phys. Status Solidi B* **79**, 713 (1977).
- <sup>37</sup>J. Y. Kim, S. M. Choi, W. S. Seo, and W. S. Cho, "Thermal and electronic properties of exfoliated metal chalcogenides," *Bull. Korean Chem. Soc.* **31**, 3225 (2010).
- <sup>38</sup>H. Guo, T. Yang, P. Tao, and Z. Zhang, "Theoretical study of thermoelectric properties of MoS<sub>2</sub>," *Chin. Phys. B* **23**, 017201 (2014).
- <sup>39</sup>R. Yan, J. R. Simpson, S. Bertolazzi, J. Brivio, M. Watson, X. F. Wu, A. Kis, T. F. Luo, A. R. H. Walker, and H. G. Xing, "Thermal conductivity of monolayer molybdenum disulfide obtained from temperature-dependent Raman spectroscopy," *ACS Nano* **8**, 986 (2014).
- <sup>40</sup>Y. Cai, J. Lan, G. Zhang, and Y. W. Zhang, "Lattice vibrational modes and phonon thermal conductivity of monolayer MoS<sub>2</sub>," *Phys. Rev. B* **89**, 035438 (2014).
- <sup>41</sup>A. Aiyiti, S. Q. Hu, C. R. Wang, Q. Xi, Z. F. Cheng, M. G. Xia, Y. L. Ma, J. B. Wu, J. Guo, Q. L. Wang, J. Zhou, J. Chen, X. F. Xu, and B. W. Li, "Thermal conductivity of suspended few-layer MoS<sub>2</sub>," *Nanoscale* **10**, 2727 (2018).
- <sup>42</sup>W. Li, J. Carrete, and N. Mingo, "Thermal conductivity and phonon line-widths of monolayer MoS<sub>2</sub> from first principles," *Appl. Phys. Lett.* **103**, 253103 (2013).
- <sup>43</sup>Y. C. Ding, M. Chen, and B. Xiao, "Anisotropy in lattice thermal conductivity tensor of bulk hexagonal-MT<sub>2</sub> (M = W, Mo and T = S and Se) by first principles phonon calculations," *RSC Adv.* **6**, 7817 (2016).
- <sup>44</sup>T. R. Kakuda, A. M. Limarga, T. D. Bennett, and D. R. Clarke, "Evolution of thermal properties of EB-PVD 7YSZ thermal barrier coatings with thermal cycling," *Acta Mater.* **57**, 2583 (2009).